Published in final edited form as:
J Am Chem Soc. 2010 October 27; 132(42): 14995–15004. doi:10.1021/ja1059747.

Probing the oxyferrous and catalytically active ferryl states of *Amphitrite ornata* dehaloperoxidase by cryoreduction and EPR/ENDOR spectroscopy. Detection of Compound I

Roman Davydov[†,§], **Robert L. Osborne**[‡,§,1], **Muralidharan Shanmugam**[†], **Jing Du**[‡], **John H. Dawson**[‡,¶,*], and **Brian M. Hoffman**[†,*]

[†]Department of Chemistry, Northwestern University, Evanston, Illinois 60208

[‡]Department of Chemistry and Biochemistry University of South Carolina, Columbia, South Carolina 29208

[¶]School of Medicine University of South Carolina, Columbia, South Carolina 29208

Abstract

Dehaloperoxidase (DHP) from *Amphitrite ornata* is a heme protein that can function both as a hemoglobin and a peroxidase. This report describes the use of 77 K cryoreduction EPR/ENDOR techniques to study both functions of DHP. Cryoreduced oxyferrous [Fe(II)-O_2] DHP exhibits two EPR signals characteristic of a peroxoferric [Fe(III)-O_2^{2-}] heme species reflecting the presence of conformational substates in the oxyferrous precursor. ^{1}H ENDOR spectroscopy of the cryo-generated substates shows that H-bonding interactions between His NεH and heme bound O_2 in these conformers are similar to those in the β-chain of oxyferrous hemoglobin A (HbA) and oxyferrous myoglobin, respectively. Decay of cryogenerated peroxoferric heme DHP intermediates upon annealing at temperatures above 180 K is accompanied by the appearance of a new paramagnetic species with an axial EPR signal with $g_\perp = 3.75$ and $g_\parallel = 1.96$ characteristic of an S=3/2 spin state. This species is assigned to Compound I (Cpd I) in which a porphyrin π-cation radical is ferromagnetically coupled with an S=1 ferryl [Fe(IV)=O] ion. This species was also trapped by rapid freeze-quench of the ambient-temperature reaction mixture of ferric [Fe(III)] DHP and H_2O_2. However, in the latter case Cpd I is reduced very rapidly by a nearby tyrosine to form Cpd ES [(Fe(IV)=O)(porphyrin)/Tyr·]. Addition of the substrate analogue 2,4,6-trifluorophenol (F_3PhOH) suppresses formation of the Cpd I intermediate during annealing of cryoreduced oxyferrous DHP at 190 K, but has no effect on the spectroscopic properties of the remaining cryoreduced oxyferrous DHP intermediates and kinetics of their decay. These observations indicate that substrate *i*) binds to oxyferrous DHP outside of the distal pocket, and *ii)* can reduce Cpd I to Cpd II [Fe(IV)=O]. These assumptions are also supported by the observation that F_3PhOH has only a small effect on the EPR properties of radiolytically cryooxidized and cryoreduced ferrous [Fe(II)] DHP. EPR spectra of cryoreduced ferrous DHP discloses the multiconformational nature of the ferrous DHP precursor. The observation and characterization of Cpds I, II, and ES in the absence and presence of F_3PhOH provides definitive evidence of a mechanism involving consecutive one-electron steps and clarifies the role of all intermediates formed during turnover.

[*]dawson@mail.sc.edu and bmh@northwestern.edu.
[§]These authors contributed equally.
[1]Robert L. Osborne is currently an NIH postdoctoral fellow at the QB3 Institute; University of California, 631 Stanley Hall; Berkeley, CA 94720.

Supporting Information Available: Additional EPR, ENDOR, and UV-Visible absorption spectra are included. This material is available free of charge via the Internet at http://pubs.acs.org.

Introduction

The terebellid polychaete *Amphitrite ornata* contains a bifunctional enzymatic globin, dehaloperoxidase (DHP)[1], which not only reversibly binds O_2, but also catalyzes the H_2O_2-dependent oxidative dehalogenation of haloaromatic substrates (Equation 1).[1] This report

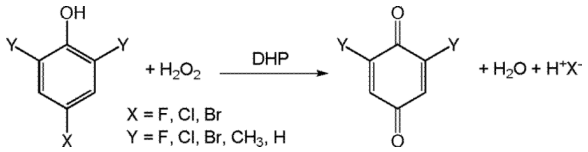

(1)

describes the use of 77 K cryoreduction EPR/ENDOR techniques to study both functions of DHP. The X-ray crystal structure of native DHP revealed that this enzyme has a protein fold analogous to that of myoglobin (Mb) and is a dimer composed of two nearly identical subunits with a total molecular weight of ~31 kDa.[2,3] The active site of DHP has consistently been characterized as one that is very similar to globins based on extensive examination using a variety of spectroscopic techniques to probe multiple oxidation states and ligand adducts of DHP.[4–7] The X-ray discovery of the presence of a substrate analogue, 4-iodophenol, in the distal pocket led to the hypothesis that DHP catalysis could involve a direct two-electron oxidation from a ferryl [Fe(IV)=O] intermediate similar to cytochromes P450. Thus, generating and characterizing the intermediate(s) of DHP that participate during substrate oxidation has been a major focus of researchers, and the mechanism has been intensely debated.[8,9]

Kinetic analyses of oxidative halophenol dehalogenation reactions catalyzed by DHP gave rates intermediate to those for the same reactions catalyzed by either horseradish peroxidase (HRP) or *Caldariomyces fumago* chloroperoxidase (CCPO) and Mb.[10–12] The voluminous data collected has led researchers to wonder whether DHP uses a strategy similar to that utilized by classical peroxidases, employing ferryl intermediates, or whether Mother Nature invoked a new strategy for this unique enzyme. The mechanism for traditional peroxidase-catalyzed reactions is well established.[13] Compound I (Cpd I) [Fe(IV)=O/porphyrin π -cation radical] forms upon reaction of the ferric [Fe(III)] heme iron with H_2O_2 (Scheme 1). The porphyrin π-cation radical of some peroxidases, like cytochrome *c* peroxidase, is rapidly reduced by an adjacent amino acid (i.e. Tyr or Trp) to form Compound ES (Cpd ES) [Fe(IV)=O/amino acid radical].[14] Cpd I/ES initiates the oxidation of most organic compounds, including phenolic substrates, by undergoing consecutive one-electron reductions to regenerate the ferric resting state of the enzyme (Scheme 1). The first one-electron transfer from substrate to Cpd I/ES generates Compound II (Cpd II) [Fe(IV)=O] with concomitant formation of a dissociable organic radical. Cpd II is subsequently reduced to the ferric enzyme by another molecule of organic substrate or by the organic radical.[13,14] However, some peroxidases can catalyze a single two-electron oxidation that involves the direct insertion of the oxygen atom from Cpd I into substrates like alkenes and thioethers yielding epoxides and sulfoxides, respectively (Scheme 1).[15–20]

Initial experiments to characterize oxidative dehalogenation reactions catalyzed by peroxidases were carried out with well-characterized enzymes such as lignin peroxidase,[21] HRP,[10,22] and CCPO.[11] The use of rapid scan stopped-flow spectroscopy confirmed that the oxidative dehalogenation reaction catalyzed by CCPO involves Cpd I and Cpd II and occurs by consecutive one-electron steps.[23] However, the inability to generate or characterize DHP Cpd I led to a number of alternate proposed mechanisms for the DHP-catalyzed oxidative halophenol dehalogenation reaction. An obligatory addition of the organic halophenol

substrate to DHP prior to H_2O_2 binding has been proposed.[5] DHP catalysis also has been posited to involve two tightly coupled one-electron steps, with the substrate remaining tightly bound until completely oxidized, with catalysis initiated only by Cpd I (i.e. not Cpd ES or Cpd II).[24] Osborne et al. recently proposed that DHP oxidizes halogenated phenols by the traditional peroxidase mechanism.[8] This hypothesis is based on the recent study where dimeric products were detected upon reaction of DHP with 4-chlorophenol and the demonstration of a catalytically active ferryl intermediate (Cpd II or Cpd ES). Despite such efforts to elucidate the DHP mechanism, DHP Cpd I has not been directly detected, although DHP Cpd ES has recently been characterized.[25]

To investigate the process of O_2 binding, we have examined EPR-active radiolytically cryoreduced and cryooxidized ferrous DHP and its Y34N mutant. The direct product of cryoreduction of oxyferrous DHP is the peroxoferric [Fe(III)-O_2^{2-}] DHP derivative, which retains the conformational state of the parent species, as well as any H-bonding interactions with moieties in the heme pocket. To characterize the DHP peroxidase function, peroxoferric DHP was annealed at temperatures above 77 K. During annealing, peroxoferric DHP becomes protonated to form hydroperoxoferric [Fe(III)-OOH^-] DHP. Upon further annealing, this species converts to enzymatically active Cpd I, which also has been trapped by rapid freeze-quench upon mixing ferric DHP with H_2O_2. EPR and ENDOR have been used to characterize all three intermediates. In the absence of the substrate analogue 2,4,6-trifluorophenol (F_3PhOH), Cpd I converts into Cpd ES; in the presence of F_3PhOH, the signal for DHP Cpd I is significantly diminished and DHP Cpd II is detected. We also find that the rate of autooxidation of oxyferrous DHP increases noticeably in the presence of F_3PhOH suggesting that substrate binding influences the properties of the active site of DHP. These studies provide the first evidence of DHP Cpd I, and the results validate a mechanism whereby DHP catalyzes the oxidative dehalogenation of halophenols by two consecutive one-electron steps initiated by Cpd I.

Materials

Potassium ferricyanide was purchased from Fluka. Primers were custom ordered (Integrated DNA Technologies). Chromatography media was purchased from either Whatman (DE-52) or BioRad (P60 size-exclusion and P6-DG desalting).

Protein Expression and Purification

Wild-type recombinant DHP and mutants were expressed in *E. coli* TB-1 cells and used for all experiments.[10] The Y34N DHP mutant was generated by site-directed mutagenesis (Qiagen) using primers encoding ~15 bases upstream and downstream of the mutation. The forward primer for the mutant is listed below with the mutation in bold. Reverse primers were complimentary: (5'-GACGAGCGCCGC**AAC**TTCAAAAACTATG).

The mutated DHP plasmid was transformed into *E. coli* TB-1 cells and purified using the Qiagen Highspeed Miniprep Kit. The Y34N DHP mutant was confirmed by automated DNA sequencing (University of South Carolina, Sequencing Facility). Wild type and Y34N DHP were purified by the same protocol. After lysis and sonication of the cell pellet, the supernatant was collected and applied to an ion exchange column equilibrated with 50 mM sodium phosphate buffer, pH 5. The reddish-brown protein was eluted with column buffer. DHP purity was calculated as the ratio of A_{416} nm/A_{280} nm (Rz). All fractions with a purity number Rz = 1.5 or greater were pooled and concentrated. DHP was further purified using a size exclusion column equilibrated with 50 mM sodium phosphate buffer, pH 5. Samples with Rz = 3.0 or greater were found to be electrophoretically homogeneous.

Sample Preparation

Isolated pure DHP exists in a mixture of ferric and oxyferrous states. Complete oxidation of the heme iron is accomplished by addition of a few crystals of potassium ferricyanide (recrystallized from water) followed by a desalting column. Protein concentrations were determined by the pyridine hemochromogen method.[26] The protein samples were concentrated and buffer-exchanged to pH 7 or pH 9 with 100 mM potassium phosphate or 50 mM Tris, respectively and were ready for experiment. The concentrated protein was stored in the − 80 °C freezer. Typical EPR samples for cryoreduction experiments contained 1 mM oxyferrous DHP in 16% glycerol/ 0.1 M KPi (pH 7) or 0.05 M Tris (pH 9). UV-Visible (UV-VIS) spectroscopy used 0.05 mM (Soret band) or 0.15 mM (visible range) DHP in 50% glycerol v/v buffer solution.

Irradiation of the frozen solutions of ferrous and oxyferrous DHP at 77 K typically was performed for 20–24 h at a rate of 0.15 Mrad/h (total dose of 3–3.5 Mrad) using a Gammacell 220 60Co unit as described previously.[27] Annealing at temperatures over the range of 77–270 K was performed by placing the sample in a bath at the desired temperature (usually *n*-pentane cooled with liquid N_2) for a desired length of time. Rapid freeze-quench experiments were performed with an Update Instruments freeze-quench apparatus fixed to rotating Cu wheels immersed in liquid N_2, on which the reaction mixture is frozen.[28] UV-VIS spectra of the cryoreduced samples in OD 4 mm quartz tubes were measured at 77 K through immersion in a liquid N_2 finger dewar with a USB 2000 spectrophotometer (Ocean optics, Inc.).

EPR and ENDOR Spectroscopy

X-band continuous wave EPR spectra were recorded on a Bruker ESP 300 spectrometer equipped with an Oxford Instruments ESR 910 continuous He flow cryostat. Q-band (35 GHz) EPR and ENDOR spectra were recorded on a modified Varian E-110 spectrometer equipped with a He immersion dewar at 2 K and operating in dispersion mode using 100 kHz field modulation under “rapid passage” conditions as described.[29] For some ENDOR measurements, the radio frequency (rf) bandwidth was broadened to 60 kHz to improve the signal-to-noise ratio.[30] EPR spectra of cryoreduced samples exhibit strong signals from free radicals created by the irradiation; this region is deleted from the spectra for clarity.

For a single orientation of a paramagnetic center, the first-order ENDOR spectrum of a proton with $I = 1/2$ in a single paramagnetic center consists of a doublet with frequencies given by equation 2. Here, ν_n is the nuclear Larmor frequency and A is the orientation-dependent

$$\nu = \nu_n + A/2 \tag{2}$$

hyperfine coupling constant of the coupled nucleus. The doublet is centered at the Larmor frequency and separated by A when $\nu_n > A/2$, as in the case for the ^1H spectra presented here. The full hyperfine tensor of the coupled nucleus can be obtained by analyzing a “2D” field-frequency set of orientation-selective ENDOR spectra across the EPR envelope, as described elsewhere.[27,32]

Results

Characterization of cryoreduced oxyferrous DHP

Figure 1 presents EPR spectra of oxyferrous DHP in 16% glycerol/buffer pH 7 upon cryoreduction at 77 K and after progressive annealing at temperatures above 77 K. The

initial EPR spectrum of 77 K cryoreduced oxyferrous DHP exhibits two EPR signals, with g tensor components characteristic of cryogenerated peroxoferric species [2.25, 2.15, ~1.97] (signal A) and [2.23, 2.12, ~1.971] (signal B) (Table 1). The spectrum resembles those previously observed with oxyferrous β HbA and Mb or α HbA-chains (Table 1).[32] The two spectroscopically distinct species A and B represent two conformers of the peroxoferric species and are indicative that the precursor oxyferrous state likewise is multiconformational. The relative intensities of the two signals is independent of the degree of cryoreduction, indicating that it is determined by the relative amounts of the two conformers of the parent diamagnetic oxyferrous DHP complex, and not by the relative probabilities of reduction of the two conformers. The relative intensity of the A conformer increases slightly at pH 9.0 (Figure 2), whereas the B conformer is almost completely eliminated in the Y34N mutant (Figure 1). The availability of the wild type enzyme, which exhibits both conformers, and a mutant that exhibits only one, allows us to distinguish the characteristics of the two conformers in ENDOR measurements discussed below.

Progressive stepwise annealing up to 185 K results in conversion of the A and B signals into a B-like signal with g = [2.24, 2.13, 1.971] (Figure 1 and Table 1). In the case of the cryoreduced oxyferrous Y34N variant, the dominant species A converts into this B-like species during annealing at 185 K. This species decays upon annealing at temperatures above 195 K. During decay of the B-like species at 195 K, a new weak transient EPR signal with g = [2.32, 2.18, 1.94] characteristic of a hydroperoxoferric species appears (data not shown); this transient is not seen during annealing at 200 K (Figure 1). At pH 9, the B-like peroxoferric intermediates convert quantitatively into the hydroperoxo intermediate (Figure 2). The lower concentration of the hydroperoxoferric intermediate achieved during 195 K annealing of cryoreduced oxyferrous DHP at pH 7 can be explained by an increased rate of proton assisted decay of this intermediate at lower pH.

Broader scans of the magnetic field show that at pH 7, the decay of the peroxoferric DHP intermediate B at 195 – 210 K is accompanied by an increase of high-spin ferric signal along with the appearance of a new species displaying an axial EPR signal with $g_{\perp} = 3.75$ and $g_{\parallel} = 1.96$ (“g 3.75 species”) (Figure 3), whose EPR signal can be detected without noticeable broadening only at temperatures below 25 K. The decay of the B-like peroxoferric species and the growth of the g 3.75 intermediate follow similar kinetics ($t_{1/2}$ ~10 min at 195 K), indicating that the peroxoferric intermediate converts into the g 3.75 species (Figure 3). The g 3.75 intermediate decays rapidly upon annealing at 225 K and this decay does not lead to the appearance of a new EPR-active species (Figure 3). The g 3.75 species also forms during decay of the g 2.32 hydroperoxoferric intermediate at pH 9, but only at higher temperatures, and it decays at temperatures above 245 K (Figure S1). At pH 9, the kinetics of formation of the g 3.75 intermediate are greatly slowed: the reaction does not occur with measurable rate at 195 K and is characterized by $t_{1/2}$ ~8 min at 215 K. This dramatic decrease of the rate of formation of the g 3.75 intermediate upon increasing the pH indicates that the process is proton assisted. This conclusion is confirmed by a significant decrease in the rate of this process in D_2O buffer at pH 9 (s*KIE* > 3) (data not shown).

The g-tensor, $g_{\perp} = 3.75$ and $g_{\parallel} = 1.96$, is characteristic of a heme having a spin S=3/2 state. This spin state has been reported for very rare examples of highly deformed ferric porphyrin complexes,[33] but also for Cpds I in which a porphyrin π -cation-radical is ferromagnetically coupled with a Fe(IV) (S=1) heme center.[31] To establish the nature of the g 3.75 intermediate, we studied the primary product forming during its decay. One can expect that the primary product of decay of Cpd I should be the EPR silent Cpd II state. Alternatively, a strained ferric heme species derived from the peroxoferric state should relax to an equilibrium ferric form with the heme-iron(III) in high spin aquo (S=5/2) or low spin hydroxo (S=1/2) states at pH < 7.5 and pH > 8.2, respectively. The absence of a new

paramagnetic species during decay of the g 3.75 species (Figure 3) indicates that this intermediate is Cpd I rather than a ferric heme. This is confirmed by the observation that cryoreduction of the EPR silent product that forms after decay of the g 3.75 intermediate results in the appearance of a new EPR active center with g = [2.44, 2.13, 1.92] characteristic of cryoreduced DHP Cpd II (Figure S2).[34] {NOTE: This signal is not generated by a second irradiation of cryoreduced ferric DHP annealed at 240 K. This observation eliminates the possibility of formation of Cpd II by a side reaction of ferric DHP with radiolytically generated H_2O_2.} Collectively, these data thus support the conclusion that the g 3.75 intermediate is Cpd I, and that it decays into an EPR silent Cpd II. This conclusion is also supported by the data of ^{1}H ENDOR spectroscopy for this intermediate presented below.

This observation prompted us to examine the possibility of forming the g 3.75 intermediate during the reaction of ferric DHP with H_2O_2 at ambient temperature. Rapid freeze-quench (RFQ) methodology was employed to trap any intermediates generated during reaction between 0.5 mM ferric DHP and 2.5 mM H_2O_2 at pH 7 and 9 with a quenching time of ~15 ms. The EPR spectrum of the resulting sample reveals two new signals in addition to that of the ferric resting state of DHP (Figure 4). One signal, the weak low-field resonance peak with a g-value of 3.75, can be assigned to Cpd I. Like the Cpd I signal generated by cryoreduction/annealing, it can only be detected at temperatures below 25 K; it also decays after annealing at 230 K. In addition, there is a very strong radical signal at g~ 2 (Figure 4). The radical signal is identical to that for the recently reported radical intermediate that was trapped during reaction of ferric DHP with H_2O_2 and assigned to a Tyr radical.[25]

The half saturation power for this radical species ($P_{1/2}$) is 0.6 mW at 18 K and is much greater than 0.00016 mW measured for TEMPO radical (Figure S3). This difference indicates the presence of magnetic interaction between the radical intermediate and a nearby paramagnetic center that causes decreasing T_1. The paramagnetic center is likely the Cpd II ferryl heme, S=1. This radical intermediate was not detected during decay of the g 3.75 intermediate formed by cryoreduction. This is likely because signals from residual radiolytically generated matrix radicals in the samples are so strong, even after annealing at 240 K for 1 min, that the new signal cannot be detected. In addition, the results of the RFQ experiment shows that the protein radical species is relatively unstable at 240 K. Incubation of the RFQ samples of DHP for 1 min at 240 K decreases of the radical signal by a factor > 50.

Effect of substrate

In these studies, F_3PhOH was used as a substrate analogue because it has better solubility than its natural substrate, 2,4,6-tribromophenol. F_3PhOH has previously been shown to be a good substrate with a turnover rate comparable to that of 2,4,6-tribromophenol.[35] In the presence of high concentrations of F_3PhOH (20 mM), the rate of autooxidation of oxyferrous DHP noticeably increases, so that samples used in the experiments contain up to 20% of the ferric form. The increased rate of autooxidation of oxyferrous DHP induced by F_3PhOH indicates a perturbing effect of the bound substrate on the oxyferrous heme moiety. However, this substrate analog has no detectable effect on the spectroscopic properties of cryoreduced oxyferrous DHP or on those of the intermediates arising during its annealing (Figure S4). This observation correlates with an absence of an observable effect of F_3PhOH on the EPR properties of the ferrous DHP–NO complex (Figure S5). In addition, F_3PhOH has no influence on the rate of decay of the peroxo- and hydroperoxoferric heme intermediates of DHP at pH 7 and 9, respectively (data not shown). In the presence of F_3PhOH, the decay of cryoreduced oxyferrous DHP is accompanied by formation of a very small amount of the g 3.75 intermediate (Figure S6). The latter at least in part is a consequence of reaction of DHP Cpd I with bound substrate. Indeed, repeated

cryoirradiation of cryoreduced oxyferrous DHP+F_3PhOH annealed at 220 K for 1 min results in the appearance of a g_1 = 2.44 EPR signal that is characteristic of cryoreduced Cpd II. This observation thus shows that during annealing, Cpd I is likely reduced to Cpd II by bound substrate. To some degree, bound substrate might favor reduction of the ferryl heme in the g 3.75 species by a nearby amino-acid residue, but the presence of a relatively strong residual radiolytically generated radical signal, even after annealing the sample at relatively high temperatures of 220–240 K, complicates detection of the resulting protein radical. This assumption also is not supported by recent kinetic studies.[25]

ENDOR of the cryogenerated oxyferrous DHP intermediates

We employed 35 GHz ENDOR spectroscopy to better characterize the cryoreduced oxyferrous DHP species and the intermediates generated during its annealing.

Cryogenerated A and B species

The orientation-selective, 2D field/frequency CW ^{1}H ENDOR pattern was collected for cryoreduced oxyferrous Y34N DHP in 16% glycerol/H_2O buffer pH 7, whose EPR spectrum is dominated by the peroxoferric species A (Figure 5). The spectra disclose a strongly coupled ^{1}H ENDOR signal with A_{max} ~17 MHz at g_1 that disappears in D_2O buffer. Such a signal has been assigned to an H-bond to the peroxoferric moiety. Numerous simulations of the field-dependent pattern lead to the best fit that employed a nearly axial hyperfine tensor with a_{iso} = 11.4 MHz (Figure S7, Table 2). Notably, the EPR signal and ^{1}H ENDOR pattern for species A are reminiscent of those reported for cryoreduced oxyferrous HbA β-chain (Table 2).[32] These similarities suggest structural similarities between the oxyferrous heme interaction with its distal surroundings in the DHP A conformer and in HbA β-chains.

The 2D field/frequency ^{1}H CW ENDOR pattern for the B-like species formed upon annealing the sample at 170 K (Figure 6) is quite different from that for the A species. We have found that the ^{1}H ENDOR pattern for the primary species B obtained by subtraction of ^{1}H ENDOR spectra for species A from the corresponding ^{1}H ENDOR spectra for cryoreduced oxyferrous DHP that contains both the A and B species is similar to that presented in Figure 6 (data not shown). Simulation of the field dependent pattern presented in Figure 6 gives a best fit with a_{iso} = 3.01 MHz, compared to a_{iso} = 11.4 MHz for the A conformer; other parameters are listed in Table 2 (Figure S8). The parameters of the B conformer are very close to those reported for the dominant peroxoferric conformer in the cryoreduced oxyferrous complex of Mb (or HbA α chains)[32] (Table 2) suggesting similar environments of the oxyferrous heme moieties in oxyferrous Mb and oxyferrous DHP conformer B.

The hydroperoxoferric DHP intermediate trapped during annealing at 210 K shows ^{1}H ENDOR spectra with maximum hyperfine coupling of $A_{max} \approx 10$ MHz characteristic of the proton of the hydroperoxo ligand coordinated to ferric heme (Figure S9).[36]

The g 3.75 signal assigned to Cpd I displays two strongly coupled nonexchangeable proton signals in D_2O with A_{max} ~10 and ~ 20 MHz, each with a nearly isotropic hyperfine coupling (Figure S10). ENDOR studies of HRP Cpd I show that these signals may be assigned to a porphyrin π-cation radical.[37] Such signals do not appear in the ENDOR of a ferric heme, and thus these measurements confirm that the g 3.75 signal is associated with Cpd I. The relatively low concentration of the g 3.75 species made it impossible to obtain useful ^{14}N ENDOR results.

Absorption spectra

We also employed UV-VIS absorption spectroscopy to study cryoreduced oxyferrous DHP at 77 K. Cryoreduction of oxyferrous DHP results in the appearance of a new Soret band at 430 nm and a significant decrease in the intensities of the blue-shifted α and β bands (Figure S11). The absorption spectrum is assigned to the peroxoferric DHP intermediate. It was obtained by subtracting the spectrum of the irradiated sample from that of the unreduced form of oxyferrous DHP and is characterized by Soret, β, and α bands at 430, 537 and 562 nm, respectively (Table 3). Comparison of this peroxoferric spectrum with those published for hydroperoxoferric intermediates of heme oxygenase and HRP, both histidine-ligated heme enzymes, shows that protonation of the peroxo ligand leads to a noticeable red-shift of the Soret band (Table 3). The absorption spectra of the hydroperoxoferric DHP intermediate and of the g 3.75 species that appears after annealing at temperatures above 200 K could not be measured because the samples become nontransparent at these temperatures.

Characterization of ferrous DHP and its interaction with substrate

Irradiation of the frozen solutions of EPR-silent ferrous hemoproteins has been previously shown to generate both one-electron oxidized and reduced species.[38] The paramagnetic species produced and trapped at 77 K retains the conformation of the ferrous precursor and can be used as an EPR probe of the structure of the EPR silent ferrous precursor.[38]

The EPR spectrum of γ -irradiated ferrous DHP, presented in Figures 7, 8 and S12, exhibits four different EPR signals from the cryo-irradiated ferrous heme. Three are generated by cryoreduction. One of these has an axial EPR signal, $g_\perp = 2.26$ and $g_\parallel = 1.933$, that is detectable at 77 K and can be assigned to Fe(I) DHP (Figure 7, S12). The $g_\parallel$ component of the signal exhibits a well-resolved 3-line pattern of superhyperfine coupling from the nitrogen of the proximal His coordinated to the Fe (I) (Figure S12). A minor peak at g ~ 3.8 is a component of the EPR signal for an S=3/2 state of cryoreduced ferrous DHP, with a porphyrin-centered radical antiferromagnetically coupled to high spin Fe(II) S=2.[38] At temperatures below 12 K, the EPR spectrum reveals the presence of a second cryogenerated Fe(I) species with more anisotropic g-tensor, $g_\perp = 2.36$ and $g_\parallel = 1.931$; it also exhibits well resolved hyperfine coupling from the proximal His nitrogen in the $g_\parallel$ feature (Figure S12). The presence of three different EPR signals associated with cryoreduced ferrous DHP is indicative of the multiconformational nature of the ferrous precursor. In addition, as discussed immediately below, a signal is seen from the cryooxidized ferrous DHP.

Addition of either 50 mM F_3PhOH or 10 mM 4-fluorophenol (4-F-PhOH) was shown to cause loss of the H_2O coordinated to the heme iron of resting ferric DHP.[39] In contrast, addition of 50 mM F_3PhOH or 10 mM 4-F-PhOH to ferrous DHP has no detectable effect on the EPR properties of the cryogenerated Fe(I) species (data not shown). This may be the result of either the low affinity of the substrate for ferrous DHP or the weak influence of the bound substrate on the spectroscopic properties of the cryogenerated Fe(I) species. Experiments with ferric DHP formed by cryooxidation of ferrous DHP allowed us to resolve this ambiguity. Cryooxidized ferrous DHP shows a rhombic EPR signal with g values of 6.46, 5.39 and ~ 2.0, characteristic of a pentacoordinated high-spin ferric heme (Figure 8, Table 4). This signal differs from that for resting high-spin ferric DHP (Figure 8, Table 4) reflecting structural differences between heme moieties in ferrous and ferric DHP.[40,41] In contrast to the influence of F_3PhOH on the cryogenerated Fe(I) DHP state, addition of F_3PhOH results in small, though reproducible, changes in the g-tensor of cryogenerated ferric DHP (Table 4, Figure 8). The absence of a detectable effect of this substrate on the EPR spectra of the cryogenerated Fe(I) species is probably due to the low sensitivity to the perturbing effect by bound substrate. Interestingly, in the presence of 10 mM 4-F-PhOH, which might bind inside the distal pocket of ferric DHP,[35] the cryogenerated ferric form

exhibits a more complicated EPR spectrum consisting of 3 signals (Table 4). The EPR signal of the dominant species A is similar to that for cryoxidized substrate-free ferrous DHP, while the two minor species B and C show distinct EPR signals (Table 4). The ferric states cryogenerated in the presence or absence of substrate relax to their equilibrium forms at temperature above 200 K. As migration of F_3PhOH from bulk solution to the heme is unlikely at this temperature, formation of a relaxed substrate-bound ferric form at 200 K confirms that F_3PhOH was bound to the ferrous precursor.

^{19}F-ENDOR of bound substrate

^{19}F ENDOR measurements on cryoreduced ferrous DHP were carried out to test whether F_3PhOH binds within the DHP heme pocket. An F-atom on the substrate that is situated within 4 Å from the heme iron is expected to show detectable ^{19}F ENDOR signals well separated from nonexchangeable ^{1}H ENDOR signals. We saw no ^{19}F ENDOR signals from cryoreduced ferrous DHP, oxyferrous DHP, and ferrous-NO DHP in the presence of F_3PhOH. This observation together with the absence of any effect of F_3PhOH on the EPR spectra of cryoreduced oxyferrous DHP, ferrous DHP, or ferrous-NO DHP is consistent with the assumption that the substrate analog binds peripherally to the heme and not in a well-defined active site.2

Discussion

Oxyferrous DHP

The crystal structure of the oxyferrous complex of C73S DHP at 100 K shows the distal histidine (His55) with a single conformation inside the distal pocket.[40] The Fe O(1)–O(2) angle is ~120° and both oxygen atoms can form H-bonds to the $N^{\varepsilon 2}$H of the distal His, with distances of 2.8 Å for $N^{\varepsilon 2}$-O(2) and 3.2 Å for $N^{\varepsilon 2}$-O(1). The present study provides insight into the active-site structure of oxyferrous DHP in solution. Cryoreduced species trapped at 77 K conserve the structure of the parent diamagnetic precursor,[32,42,43] and therefore can be used as sensitive EPR probes for studying structural features of the oxyferrous heme moiety. The presence of two paramagnetic species with distinct spectroscopic properties in cryoreduced oxyferrous DHP indicates the presence of two conformational substates in the oxyferrous precursor. This observation is similar to that reported for cryoreduced oxyferrous β- and α-chains of Hb A.[32] The fact that the shape of the EPR signal of oxyferrous DHP is independent of the degree of cryoreduction indicates that the relative amounts of cryogenerated species A and B reflect the relative populations of the conformational substates in the oxyferrous DHP precursor.[32] The populations of substates A and B in oxyferrous DHP slightly depend on pH and are significantly modulated by the Y34N DHP mutation (see Figure S13 to see the location of Y34). One of the possible reasons for the differences between the crystal structure obtained at 100 K and that in solution may be that crystallization selects a single conformational substate. Structural heterogeneity also has been reported for the active site of the ferrous-CO DHP complex in solution, which shows multiple stretching bands of heme-bound CO.[44]

EPR and ^{1}H ENDOR reveal how the properties of cryogenerated peroxoferric intermediates are modulated by H-bonds to the peroxo ligand as well as by electrostatic interactions between the ligand and distal pocket surrounding.[32,45–47] Notably, the spectroscopic properties of the two cryogenerated DHP peroxoferric intermediates A and B differ

[2]Abbreviations: DHP, dehaloperoxidase; Cpd I, Compound I; Cpd II, Compound II; Cpd ES, Compound ES; Mb, horse heart myoglobin; HRP, horseradish peroxidase; CCPO, *Caldariomyces fumago* chloroperoxidase; F_3PhOH, 2,4,6-trifluorophenol; EPR, electron paramagnetic resonance; ENDOR, electron nuclear double resonance; RFQ, rapid freeze quench; UV-VIS, UV-visible; Histidine, His.

substantially, respectively resembling those previously reported for the dominant species in cryoreduced oxyferrous Hb β -chain and oxyferrous Mb (or oxyferrous Hb α-chain), (Tables 1 and 2), indicating structural similarities between the H-bonds to the bound O_2 molecule in the respective proteins. The crystal structure of cryogenerated peroxoferric Mb, which is very similar to that of oxyferrous Mb, revealed a strong H-bond interaction between distal His 64 $N^{\varepsilon}H$ and the distal oxygen atom (N-O distance ~2.8 Å) and a much weaker interaction between this group and the proximal oxygen atom (N-O distance ~4.5 Å).[42,43] Interestingly, at a resolution of 1.25 Å, some positional disorder of His 64 was noted.[43] The 1.25 Å resolution crystal structure of oxyferrous HbA demonstrates a strong H-bond interaction between the distal His and bound O_2 in the α-chain (Nε-distal O distance ~2.7 Å) while the H-bond made by the distal His in the oxyferrous Hb β-chain is much weaker than that made by the distal His in the Hb α-chain.[48] As in the cryoreduced globins, the strongly coupled exchangeable ^{1}H ENDOR signals from the cryotrapped peroxoferric species of DHP can be assigned to an H-bond from the distal His $N^{\varepsilon}H$ to the distal oxygen of the peroxo ligand.

Ferrous DHP. Localization of bound substrate

Cryogenerated ferric and Fe(I) DHP species retain the conformation of the ferrous precursor, and are good EPR probes for the EPR-silent ferrous state. Cryoreduced ferrous DHP exhibits three distinct EPR signals that are similar to those seen in cryoreduced ferrous Mb.[38] This indicates the presence of at least three spectroscopically distinct conformational substates in the ferrous precursor. Approximate integrations indicate that the populations of g_1 3.8 and g_1 2.36 conformers are significantly less than that for the g_1 2.26 species. Likewise, the recently reported crystal structure of ferrous DHP shows two solvent-exposed conformations of the distal histidine (His55), with nitrogens more than 9.5 Å away from the heme iron. Although those differences likely would not influence the EPR spectrum the spectroscopic and X-ray results, thus both demonstrate that the ferrous DHP heme center is conformationally flexible.

Cryogenerated ferric DHP shows a much more rhombic high-spin EPR signal than that for the resting ferric state (Table 4) reflecting structural differences between heme centers in equilibrium ferric and ferrous states.[41] The spectroscopic difference cannot be explained by just the absence of the distal water ligand in the coordination sphere of cryogenerated ferric DHP because a similar difference was observed for cryogenerated and resting pentacoordinate ferric states of DHP in the presence of F_3PhOH (Table 4). Addition of F_3PhOH was shown to displace the water ligand in ferric DHP forming a pentacoordinate ferric heme center.[39] Cryooxidized ferrous Mb, which is thought to be similar to DHP, shows an almost axial EPR signal with $g_{\perp} \approx 5.9$ indicating some structural differences between ferrous heme moieties in these proteins. Numerous subtle structural effects were shown to influence the g values of the ferric heme.[33,38,49]

The first crystal structure of substrate-bound ferric DHP revealed that 4-iodophenol binds in the distal pocket but is not coordinated to the heme iron (Figure S13). To date, substrate binding has been studied by FTIR,[44] NMR, and EPR. Addition of F_3PhOH to ferric DHP leads to loss of the heme-bound water molecule[39] suggesting that the substrate binds inside the distal pocket. NMR studies performed by Franzen and coworkers have suggested two different modes of substrate interaction in the six coordinate complex of ferric DHP with CN^-. Under physiologically relevant conditions, mono- and dihalophenols bind inside the heme pocket while trihalophenols interact with the protein at an external site to the distal pocket.[35] However, FTIR studies showed that F_3PhOH can bind inside the distal pocket of the CO complex of ferrous DHP at cryogenic temperatures but no binding of this substrate was observed at temperatures above 260 K.[44] On the basis of comparison of the reactivity of mono-, di- and trihalogenated substrates, Franzen et al. drew the conclusion that the active

site for substrate oxidation in DHP is an external site, as observed in other heme peroxidases.[35] Similarly, a recent study that examined the binding sites of monohalophenol inhibitors and natural substrates supports substrate binding peripheral to the active site.[50]

Our data on the effect of F_3PhOH on the spectroscopic properties of ferrous DHP and its complexes with O_2 and NO are consistent with this conclusion. These include the lack of detectable effects of F_3PhOH on the spectroscopic properties of the ferrous-NO DHP complex or on cryoreduced oxyferrous DHP, and the absence of ENDOR features from ^{19}F in all samples containing the substrate. The latter indicates that the distances between F atoms of the bound substrate and paramagnetic center is over 5 Å. Qualitatively similar results were obtained for ferrous DHP. The fact that the g 3.75 species assigned to Cpd I does not accumulate during annealing of cryoreduced oxyferrous DHP in the presence of F_3PhOH suggested reduction of this intermediate by the bound substrate; the resulting formation of Cpd II is confirmed during repeated cryoirradiation.

Detection and characterization of reactive intermediates through annealing of cryoreduced oxyferrous complexes

The data reported herein show that when the cryogenerated peroxoferric A and B intermediates of DHP are annealed at temperatures above 170 K, they relaxe to the B-like conformational substate. The B-like species accepts a proton at temperatures above 180 K to form the hydroperoxoferric intermediate (Scheme 2), (Cpd 0), which is well-known as a key intermediate in the catalytic cycles of heme-containing monooxygenase and peroxidase enzymes. This state, which accumulates during annealing when pH > 8, is converted in a proton-assisted manner into the g 3.75 species assigned to Cpd I, whose S = 1 ferryl ion is ferromagnetically coupled to the porphyrin π-cation radical. As noted above, the low concentration of the transient hydroperoxoferric species in the annealing pattern of cryoreduced oxyferrous DHP at pH 7.0 (Figure 1) is likely due to the significant increase in the rate of proton assisted conversion of this intermediate into Cpd I at higher proton concentration. During the reaction of ferric DHP with H_2O_2 at ambient temperature, we also observed the formation of Cpd I, which rapidly converted to Cpd ES.

However, no Cpd ES was detected during the decay of the Cpd I generated upon annealing of cryoreduced oxyferrous DHP, although we could observe formation of Cpd II during this process. As noted above, this can be because signals from residual radiolytically generated matrix radicals in the samples are so strong, as well as the relatively low stability of Cpd ES at temperatures above 230 K.

A significant decrease in Cpd I formation was observed during annealing of cryoreduced oxyferrous DHP prepared in the presence of F_3PhOH, even though this substrate has no visible effect on the decay kinetics of the cryogenerated peroxoferric or hydroperoxoferric intermediates. The most likely explanation for this is electron transfer from substrate to form Cpd II and the substrate radical. Formation of Cpd II was confirmed by repeated cryoirradiation of the sample. The F_3PhOH radical could not be detected because of the presence of strong signals from the residual radiolytically generated radicals.

In this study, we have successfully generated and characterized DHP Cpd I in the absence and presence of F_3PhOH and this has enabled us to clarify numerous mechanistic ambiguities for the DHP-catalyzed oxidative dehalogenation of halophenols. The data presented herein led to the following conclusions: *i*) Cpd I along with Cpd ES can participate in the reaction with substrate and the contribution of Cpd I in this process is expected to increase with substrate concentration; *ii*) the substrate binds to oxyferrous DHP, probably close to the heme, but outside of the distal side of the heme pocket as observed in other heme peroxidases. The formation of Cpd II during the process suggests that the

reaction with Cpd I likely occurs through two consecutive one-electron oxidations of substrate, consistent with the results of other kinetic studies:[8] the first oxidation yields a dissociable organic radical and Cpd II instead of a single two-electron oxidation mechanism involving direct insertion of oxygen of Cpd I into substrate molecule, which could be more favorable if substrate was localized inside of the distal site of the heme pocket.

Supplementary Material

Refer to Web version on PubMed Central for supplementary material.

Acknowledgments

This work was supported by the NIH (HL13531, BMH) and NSF (MCB 0820456; JHD). RLO gratefully acknowledges support from an NIH Postdoctoral Fellowship (GM 820952). We are grateful to Prof. H. Halpern (University of Chicago) for providing access to the Gammacell 60Co source.

References

1. Chen Y-P, Woodin SA, Lincoln DE, Lovell CR. J. Biol. Chem. 1996; 271:4609–4612. [PubMed: 8617721]
2. LaCount MW, Zhang EL, Chen Y-P, Han KP, Whitton MM, Lincoln DE, Woodin SA, Lebioda L. J. Biol. Chem. 2000; 275:18712–18716. [PubMed: 10751397]
3. Lebioda L, LaCount MW, Zhang E, Chen Y-P, Han KP, Whitton MM, Lincoln DE, Woodin SA. Nature. 1999; 401:445. [PubMed: 10519547]
4. Roach MP, Chen Y-P, Woodin SA, Lincoln DE, Lovell CR, Dawson JH. Biochemistry. 1997; 36:2197–2202. [PubMed: 9047320]
5. Franzen S, Roach MP, Chen Y-P, Dyer BR, Woodruff WH, Dawson JH. J. Am. Chem. Soc. 1998; 120:4658–4661.
6. Osborne RL, Sumithran S, Coggins MK, Chen Y-P, Lincoln DE, Dawson JH. J. Inorg. Biochem. 2006; 100:1100–1108. [PubMed: 16603247]
7. Belyea J, Belyea CM, Lappi S, Franzen S. Biochemistry. 2006; 36:2197–2202.
8. Osborne RL, Coggins MK, Raner GM, Walla M, Dawson JH. Biochemistry. 2009; 48:4231–4238. [PubMed: 19371065]
9. Belyea J, Gilvey LB, Davis MF, Godek M, Sit TL, Lommel SA, Franzen S. Biochemistry. 2005; 44:15637–15644. [PubMed: 16313166]
10. Osborne RL, Taylor LO, Han KP, Ely B, Dawson JH. Biochem. Biophys. Res. Commun. 2004; 324:1194–1198. [PubMed: 15504340]
11. Osborne RL, Raner GM, Hager LP, Dawson JH. J. Am. Chem. Soc. 2006; 128:1036–1037. [PubMed: 16433494]
12. Osborne RL, Coggins MK, Walla M, Dawson JH. Biochemistry. 2007; 46:9823–9829. [PubMed: 17676875]
13. Dawson JH. Science. 1988; 240:433–439. [PubMed: 3358128]
14. Pond, AE.; Ledbetter, AP.; Sono, M.; Goodin, DB.; Dawson, JH. Part I, Biological Systems. In: Gray, HB.; Winkler, JR.; Balzani, V., editors. Electron Transfer in Chemistry. Vol. vol. III. Wiley VCH Publishers; Weinheim, Germany: 2001. p. 56-104.
15. McCarthy M-B, White RE. J. Biol. Chem. 1983; 258:9153–9158. [PubMed: 6874682]
16. Kedderis GL, Rickert DE, Pandey RN, Hollenberg PF. J. Biol. Chem. 1986; 261:15910–15914. [PubMed: 3782097]
17. Kobayashi S, Nakano M, Goto T, Kimura T, Schaap AP. Biochem. Biophys. Res. Commun. 1986; 135:166–171. [PubMed: 3954766]
18. Kobayashi S, Nakano M, Kimura T, Schaap AP. Biochemistry. 1987; 26:5019–5022. [PubMed: 3663642]

19. Ortiz de Montellano PR, Choe YS, DePillus G, Catalano CE. J. Biol. Chem. 1987; 262:11641–11646. [PubMed: 3624229]
20. Zhang R, Nagraj N, Lansakara-P. DSP, Hager LP, Newcomb M. Org. Lett. 2006; 8:2731–2734. [PubMed: 16774243]
21. Hammel KE, Tardone PJ. Biochemistry. 1988; 27:6563–6568.
22. Ferrari RP, Laurenti E, Trotta F. J. Biol. Inorg. Chem. 1999; 4:232–237. [PubMed: 10499096]
23. Osborne RL, Coggins MK, Terner J, Dawson JH. J. Am. Chem. Soc. 2007; 129:14838–14839. [PubMed: 17990879]
24. Franzen S, Gilvey LB, Belyea JL. Biochem. Biophys. Acta. 2007; 1774:121–130. [PubMed: 17182294]
25. a) Feducia J, Dumarieh R, Gilvey LBG, Smirnova T, Franzen S, Ghiladi RA. Biochemistry. 2009; 48:995–1005. [PubMed: 19187035] b) D'Antonio J, D'Antonio EL, Thompson MK, Bowden EF, Franzen S, Smirnova T, Ghiladi RA. Biochemistry. 2010; 49:6600–6616. [PubMed: 20545299]
26. Paul K-G, Theorell H, Åkeson Å . Acta Chem. Scand. 1953; 7:1284–1287.
27. Davydov R, Makris TM, Kofman V, Werst DE, Sligar SG, Hoffman BM. J. Am. Chem. Soc. 2001; 123:1403–1415. [PubMed: 11456714]
28. Lin Y, Gerfen GJ, Rousseau DL, Yeah SR. Anal. Chem. 2003; 75:5381–5386. [PubMed: 14710815]
29. Werst MM, Davoust CE, Hoffman BM. J. Am. Chem. Soc. 1991; 113:1533–1538.
30. Hoffman BM, Derose VJ, Ong JL, Davoust CE. J. Magn. Reson. Ser. A. 1994; 110:52–57.
31. a) Benecky MJ, Frew JE, Scowen N, Jones P, Hoffman BM. Biochemistry. 1993; 32:11929–11933. [PubMed: 8218266] b) Patterson WR, Poulos TL, Goodin DB. Biochemistry. 1995; 34:4342–4345. [PubMed: 7703248]
32. (a) Davydov R, Kofman V, Nocek JM, Noble RW, Hui H, Hoffman BM. Biochemistry. 2004; 43:6330–6338. [PubMed: 15147217] (b) Hoffman BM. Acc. Chem. Res. 1991; 24:164–170.
33. Sakai T, Ohgo Y, Ikeue T, Takahashi M, Takeda M, Nakamura M. J. Am. Chem. Soc. 2003; 125:13028–13029. [PubMed: 14570467]
34. Davydov R, Osborne RL, Kim SH, Dawson JH, Hoffman BM. Biochemistry. 2008; 47:5147–5155. [PubMed: 18407661]
35. Davis MF, Gracz H, Vendeix FAP, deSerrano V, Somansundaram A, Decatur SM, Franzen S. Biochemistry. 2009; 48:2164–2172. [PubMed: 19228049]
36. Davydov R, Kofman V, Fujii H, Yoshida T, Ikeda-Saito M, Hoffman BM. J. Am. Chem. Soc. 2002; 124:1798–1808. [PubMed: 11853459]
37. Roberts JE, Hoffman BM, Rutter R, Hager LP. J. Biol. Chem. 1981; 256:2118–2121. [PubMed: 6257699]
38. Davydov R, Hoffman BM. J. Biol. Inorg. Chem. 2008; 13:357–369. [PubMed: 18058139]
39. Smirnova TI, Weber RT, Davis MF, Franzen S. J. Am. Chem. Soc. 2008; 130:2128–2129. [PubMed: 18217756]
40. deSerrano V, Chen Z, Davis MF, Franzen S. Acta Cryst. 2007; D63:1094–1101.
41. Chen Z, deSerrano V, Betts L, Franzen S. Acta Cryst. 2009; D65:34–40.
42. Unno M, Chen H, Kusama S, Shaik S, Ikeda-Saito M. J. Am. Chem. Soc. 2007; 129:13394–13395. [PubMed: 17929929]
43. Hersleth H-P, Hsiao Y-W, Ryde U, Görbitz CH, Anderson KK. Biochem. J. 2008; 412:257–264. [PubMed: 18215120]
44. Nienhaus K, Deng P, Belyea J, Franzen S, Nienhaus GU. J. Phys. Chem. 2006; B110:13264–13276.
45. Davydov R, Satterlee JD, Fujii H, Sauer-Masarwa A, Busch DH, Hoffman BM. J. Am. Chem. Soc. 2003; 125:16340–16346. [PubMed: 14692776]
46. Davydov R, Chauhan N, Thackray SJ, Anderson JLR, Papadopoulou ND, Mowat CG, Chapman SK, Raven EL, Hoffman BM. J. Am. Chem. Soc. 2010; 132:5494–5500. [PubMed: 20353179]
47. Silaghi-Dumitrescu R, Cooper CE. Dalton Trans. 2005:3477–3482. [PubMed: 16234928]

48. Park S-Y, Yokoyama T, Shibayama N, Shiro Y, Tame JRH. J. Mol. Biol. 2006; 360:690–701. [PubMed: 16765986]

49. a) Jakopitsch C, Obinger C, Un S, Ivanchich A. J. Inorg. Biochem. 2006; 100:1091–1099. [PubMed: 16574230] b) Hu C, Sulok CD, Paulat F, Lehnert N, Twigg AI, Hendrich MP, Schulz CE, Scheidt WR. J. Am. Chem. Soc. 2010; 132:3737–3750. [PubMed: 20192189]

50. Davis MF, Bobay BG, Franzen S. Biochemistry. 2010; 49:1199–1206. [PubMed: 20067301]

51. Denisov IG, Ikeda-Saito M, Yoshida T, Sligar SG. FEBS Lett. 2002; 532:203–206. [PubMed: 12459490]

52. Denisov IG, Makris TM, Sligar SG. J. Biol. Chem. 2002; 277:4706–4710.

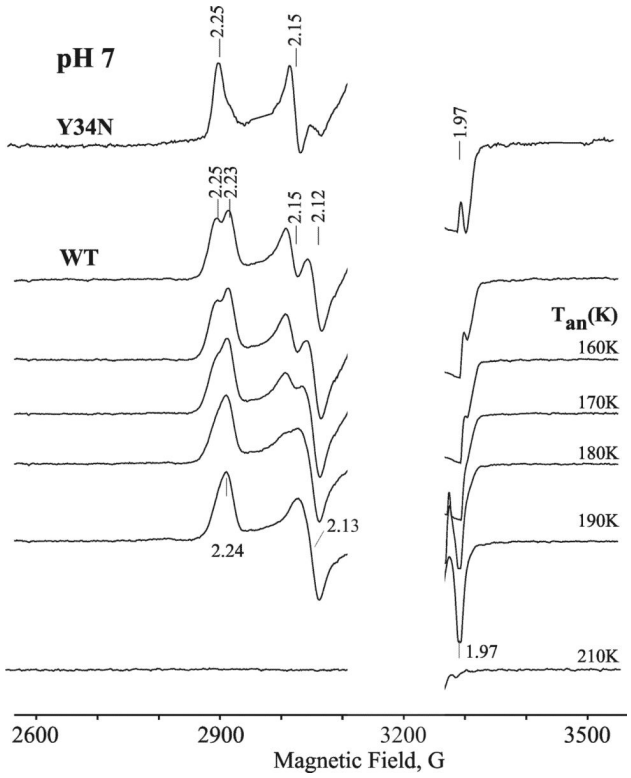

Figure 1.

EPR spectra of cryoreduced oxyferrous Y34N DHP and cryoreduced oxyferrous wild type DHP in 16% glycerol/0.1 M potassium phosphate buffer, pH 7, annealed at indicated temperatures. Species A discussed in text has $g_1 = 2.25$, species B has $g_1 = 2.23$ (Table 1). Conditions: T = 25 K; microwave power = 10 mW; modulation amplitude = 5 G; microwave frequency = 9.38 GHz.

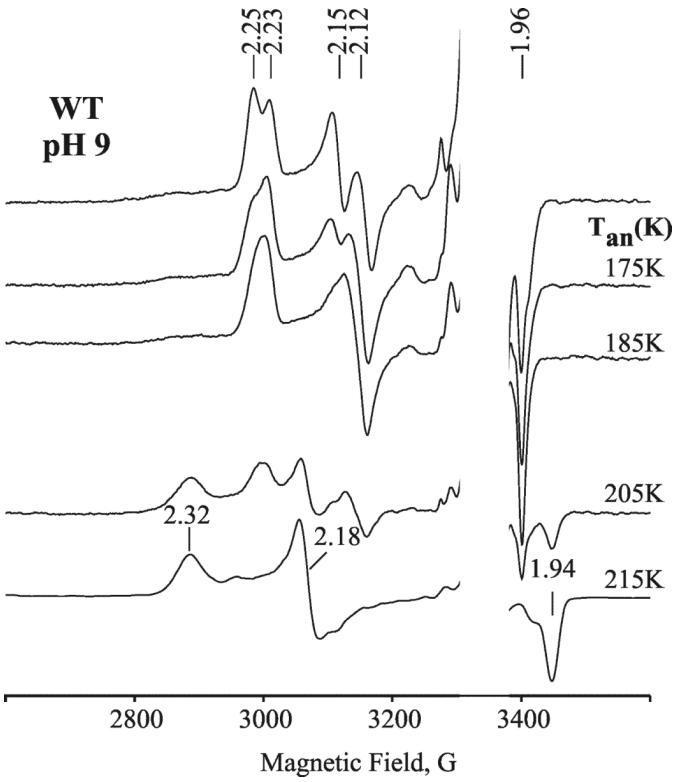

Figure 2.
EPR spectra of cryoreduced oxyferrous wild type DHP in 16% glycerol/0.05 M Tris buffer, pH 9, annealed at indicated temperatures. Conditions: T = 25 K; microwave power = 10 mW; modulation amplitude = 5 G; microwave frequency = 9.38 GHz.

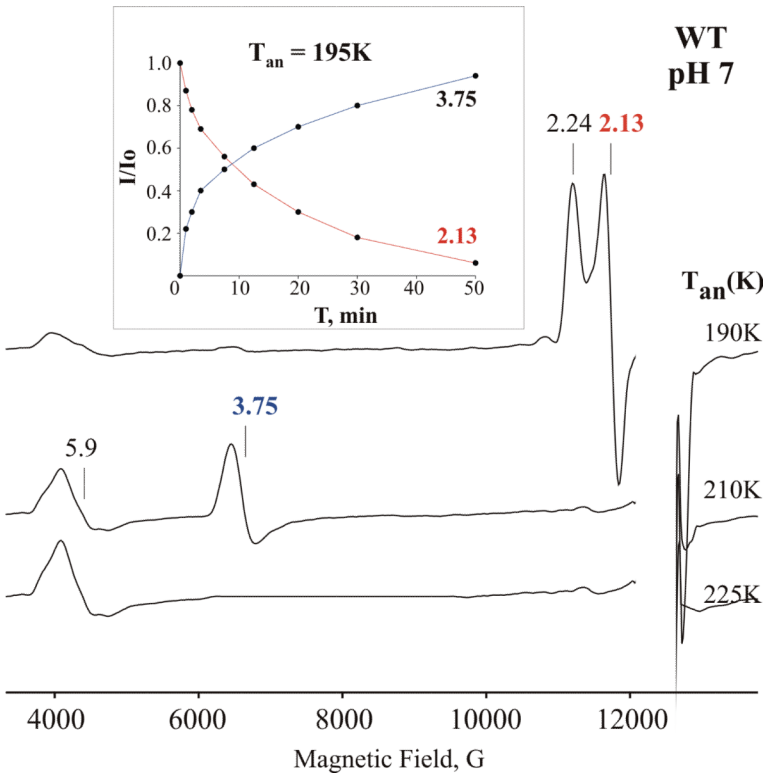

Figure 3.

2 K Q-band EPR spectra of cryoreduced oxyferrous DHP in 16% glycerol/ 0.1 M potassium phosphate buffer, pH 7, after stepwise annealing at 190 – 225 K for 1 min. Inset: kinetic decay of peroxoferric DHP intermediate (g_1 2.24 species) and growth of g 3.75 intermediate at 195 K. Conditions: T = 2 K; microwave power = 20 μW; modulation amplitude = 1 G; microwave frequency = 34.99 GHz.

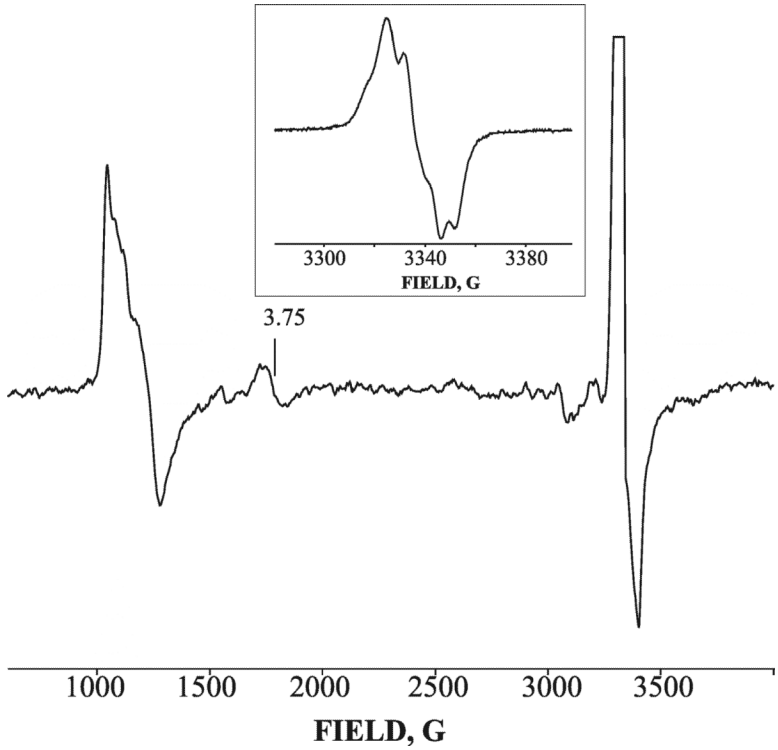

Figure 4.

EPR spectra of intermediates arising during the reaction between 0.5 mM ferric DHP and 2.5 mM H_2O_2 in 0.05 M Tris buffer, pH 9, rapid freeze-quenched in 15 ms. Inset: EPR spectrum of radical species arising during this reaction. Conditions: T = 8 K; microwave power = 10 mW; modulation amplitude = 10 G; Microwave frequency = 9.38 GHz. Inset: T = 25 K; microwave power = 0.1 mW; modulation amplitude = 3 G.

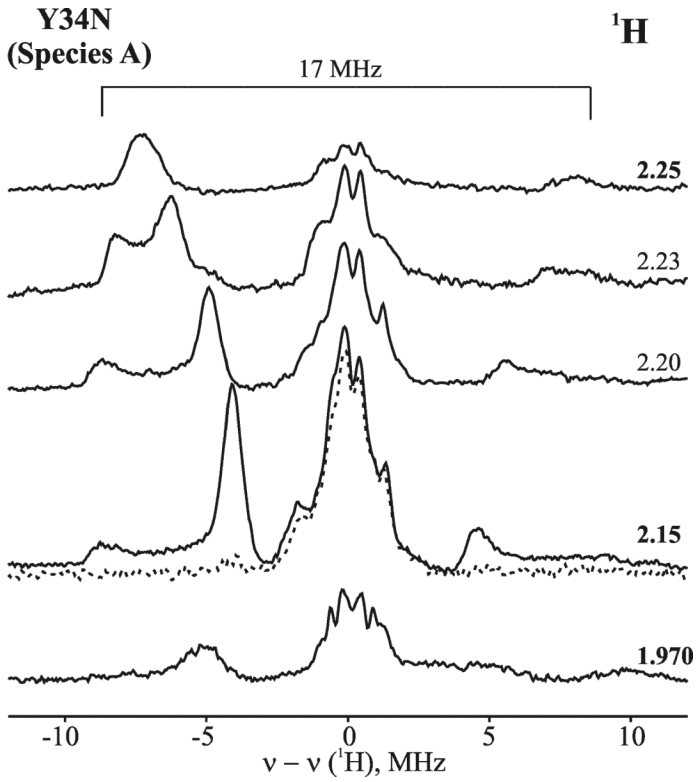

Figure 5.

2D frequency/field ^{1}H ENDOR spectra of cryoreduced oxyferrous Y34N DHP in 16% glycerol-H_2O/0.1 M potassium phosphate buffer, pH 7, (species A) (solid line) and in d_3-glycerol-D_2O/0.1 M potassium phosphate buffer, pD 6.6 (dotted line). Conditions: T = 2 K; microwave frequency = 34.99 MHz; modulation amplitude = 2 G; scan rate = 0.5 MHz/s; rf power = 7 W; frequency bandwidth = 60 kHz.

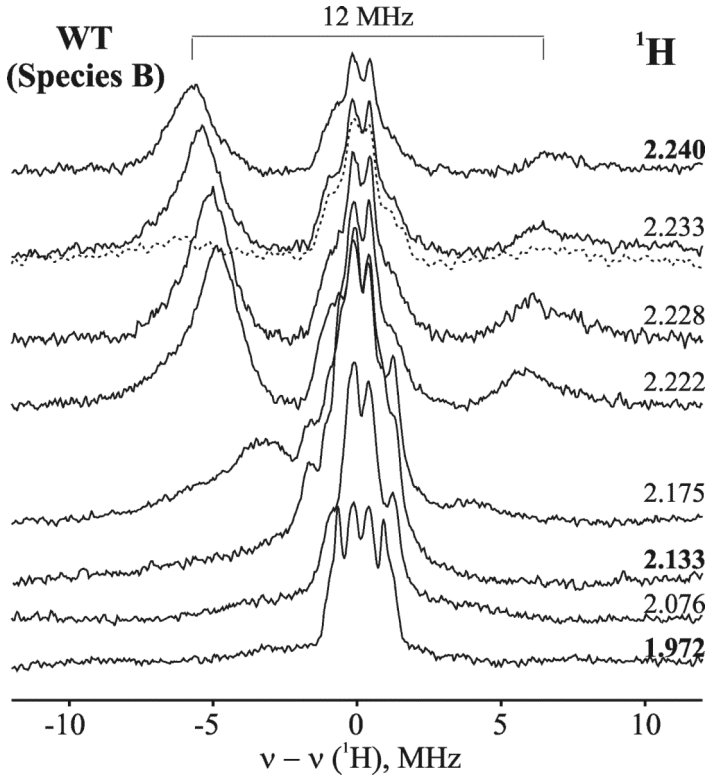

Figure 6.

2D frequency/field ^{1}H CW ENDOR spectra of cryoreduced oxyferrous DHP in 16% glycerol-H_2O/0.1 M potassium phosphate buffer, pH 7, annealed at 189 K for 1 min (the B species) (solid line) and in d_3-glycerol-D_2O/0.1 M potassium phosphate buffer, pH 6.6 (dashed line). Conditions are the same as described in Figure 5.

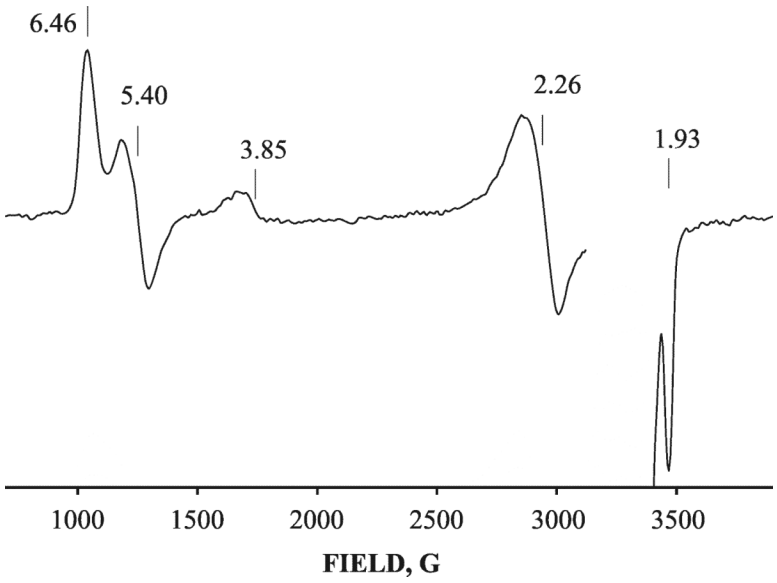

Figure 7.

EPR spectrum of 1 mM ferrous DHP in 15% glycerol/0.1 M potassium phosphate buffer, pH 7, exposed to γ-irradiation (dose of 1.9 Mr) at 77 K. Conditions: T = 14 K; microwave power = 2 mW; modulation amplitude = 10 G; microwave frequency = 9.382 GHz.

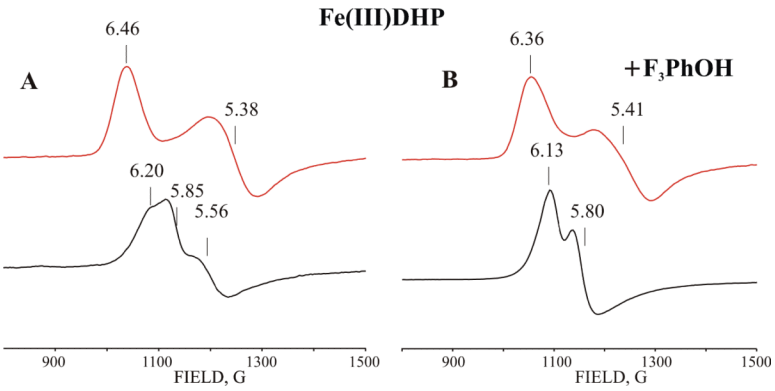

Figure 8.

Low field X-band EPR spectra of cryogenerated (red) and resting high-spin ferric forms (black) of DHP in the absence of substrate (A) and in the presence of 50 mM F_3PhOH in 20% glycerol/0.1 M potassium phosphate buffer, pH 7. Conditions: T = 8 K; modulation amplitude = 10 G; microwave power = 10 mW; microwave frequency = 9.38 GHz.

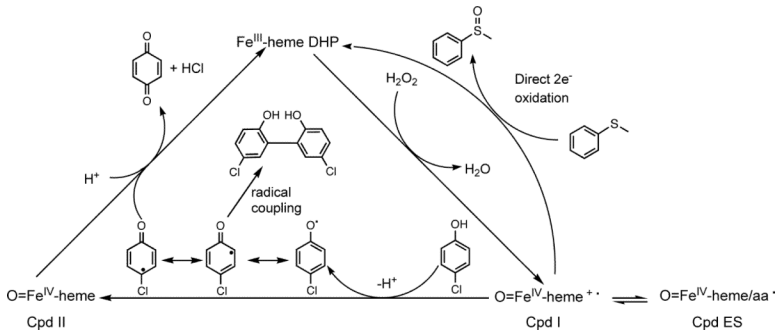

Scheme 1.

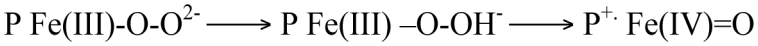

Scheme 2.

Table 1

EPR properties of cryoreduced oxyferrous DHP and oxyferrous globins.

Protein	Tan	g_1	g_2	g^3	T_{obs} (K)
Oxyferrous DHP (pH 7,9) A		2.25	2.15	1.963	77
Oxyferrous DHP (pH 7,9) B		2.23	2.12	1.971	77
	185 K	2.24	2.13	1.971	77
(pH9)	210K	2.32	2.18	1.945	77
	220–230 K	3.75	3.75	1.96	<25
Oxyferrous Hb β-chain (pH 8)[a]					
Peroxoferric Hb β-chain A		2.25	2.15	1.966	77
Peroxoferric Hb β-chain B		2.22	2.13	1.970	77
Hydroperoxoferric Hb β-chain	200 K	2.31	2.19	1.948	77
Oxyferrous Hb α-chain		2.213	2.121	1.968	77
Oxyferrous Mb		2.218	2.118	1.966	77

[a] Hb and Mb data, ref 32

Table 2

^{1}H Hyperfine interaction parameters for the exchangeable H-bond proton.

Species/signal	a_{iso}(MHz)	A_1	A_2	A_3	θ (deg)	Ψ (deg)
Oxyferrous DHP						
Peroxoferric DHP						
A	11.4	8.2	7.6	18.6	55	0
B	3	−1.45	−1.45	12.06	80	25
Oxyferrous Hb β-chain[a]	11.8	8.2	8.5	18.8	37	0
Oxyferrous Mb[a]	2.9	−1.5	−1.5	11.6	83	0

a) Hb and Mb data, Ref 32

J Am Chem Soc. Author manuscript; available in PMC 2011 October 27.

Table 3

Absorption spectra of oxyferrous DHP, peroxoferric DHP, and hydroperoxoferric intermediates of HO and HRP at 77 K.

Species	Soret	β	α	Ref
Oxyferrous DHP	417	539	577	
Peroxoferric DHP	430	537	562	
Hydroperoxoferric HO	421	530	556	(51)
Hydroperoxoferric HRP	419	526	556	(52)

Table 4

g-values of EPR signals for resting and cryogenerated ferric forms of DHP

Protein	g_1	g_2	g_3
Fe(III) DHP (pH7)	6.16	5.56	2.0
	5.85	5.85	2.0
(pH9)	2.59	2.19	1.83
	6.16	5.56	2.0
	5.85	5.85	2.0
Fe(III) DHP +4-F-PhOH (pH7– 9)	6.14	5.8	2.0
Fe(III) DHP+4-F-PhOH pH7	6.15	5.58	2.0
Cryooxidized Fe(II) DHP (pH 7–9)	6.46	5.39	nd
Cryooxidized Fe(II) DHP+F_3PhOH	6.38	5.49	nd
Cryooxidized Fe(II) DHP+4-F-PhOH	(A) 6.48	5.39	Nd
	(B)6.51	5.27	Nd
	(C) 6.21	5.62	Nd